Juan Vielma
Professor, Departamento de
Estructuras. Barquisimeto,
Univesidad Centroccidental
Lisandro Alvarado, Venezuela

Alex H. Barbat
Professor, Technical
University of Catalonia,
Barcelona, Spain

Sergio Oller
Professor, Technical
University of Catalonia,
Barcelona, Spain

ice
Institution of Civil Engineers

Seismic performance of waffled-slab floor buildings

J. Vielma MSc, PhD, A. H. Barbat PhD and S. Oller PhD

The codes used in seismic design of waffled-slab floors buildings (WSFB), such as the Spanish NCSE-02 earthquake-resistant design code, assign them restricted ductility, utilise linear structural analysis based on modal analysis, but also consider the structural ductility concept. Uncertainties arise whenever these codes are applied to the special case of buildings with waffled-slab floors, the ductility of which is doubtful. In many cases, during earthquakes, buildings with restricted ductility are unable to reach the ductility values assumed in the design process, although they may exhibit adequate values of overstrength. This paper therefore studies typical WSFB by applying static incremental non-linear analysis procedures (pushover analysis) in order to calculate their actual structural ductility and overstrength values. Fragility curves corresponding to different damage states and damage probability matrices are also calculated and compared with those of moment-resisting frame buildings (MRFB) in order to obtain useful conclusions for earthquake resistant design. One of the most relevant conclusions of this article is that the use of a better confinement and of ductile steel can only improve the seismic behaviour of MRFB but not that of WSFB.

1. INTRODUCTION

Studies performed recently in areas of Spain with low-to-moderate seismic hazard[1] reveal that seismic vulnerability is high in such areas and, consequently, that their seismic risk is significant. This is mainly owing to the typology of the existing buildings, most of them with unreinforced masonry structures, designed and built without the consideration of any earthquake-resistant criteria.[2,3] Moreover, most of the existing reinforced concrete (RC) buildings are not moment-resisting frames, but structures with waffled-slab floors.[4] It therefore appears to be useful to perform more detailed studies of this typology of buildings in order to establish if it is reasonable to recommend their use in seismic areas.

The emergence of performance-based procedures for the design and retrofit of earthquake-resistant buildings[5–7] has sparked research on the non-linear static response of buildings.[8] Among the most studied structural typologies is that of the moment-resisting frame buildings (MRFB).[9,10] However, the non-linear response of restricted ductility buildings, that is, buildings expressly designed to have low ductility, including columns-and-slabs RC buildings, has not been studied at large.[11,12] These last classes of buildings are frequent in Spain and in other European countries (e.g. Turkey) or Latin America (e.g. Ecuador, Dominican Republic and Mexico), where their waffled-slab floor version is used. It is worth mentioning that the Uniform Building Code (UBC)-97[13] and International Building Code (IBC)-2003[14] codes, as well as the Eurocode 8,[15] do not make any reference to waffled-slab floors as possible structural elements to be used in the earthquake-resistant design of buildings.

Adequacy of the response of a structure to a given seismic threat can be evaluated, in a simplified way, through examination of two important non-linear response characteristics

(a) the maximum ductility value reached by such buildings during a strong ground motion
(b) the reduction factor applied to design spectrum ordinates in order to calculate the seismic design forces, this factor being closely related to the overstrength.

According to the Norma de Construction Sismorresistente (NCSE)-02 Spanish earthquake-resistant design code,[16] waffled-slab floors buildings (WSFB) have restricted ductility values of two. This value is set based on the well-known premise that this structural typology has low capacity for energy dissipation. At the same time, apart from the UBC-97 and IBC-2003, the Eurocode 8 and NCSE-02 Spanish code do not refer directly to overstrength values, which are very important for determining the response reduction factors.[17,18]

With these observations as a starting point, the main objective of this paper is to study the typical WSFB seismic behaviour by calculating their actual structural ductility and overstrength values, using an incremental non-linear static analysis procedure (pushover analysis). In this simplified analysis, lateral forces corresponding to the first vibration mode shape are gradually applied and global structural damage indexes are used to determine the ultimate drift values of the buildings. Drift values corresponding to the yielding point are obtained by using the idealised bilinear form of the capacity curve proposed by Park.[19] The benefits of the ductility of the steel reinforcements and of the longitudinal and transversal

confinements are also evaluated using the building pushover response.

With the objective of elucidating how structural typology and design have an influence on the global response of building structures, three buildings with different characteristics were designed and analysed. The first building has waffled-slab floors and has been designed with a reduction factor of two. The second building, has moment-resisting RC frames, it is designed according to the Instruccion de Hormigon Estructura (EHE)[20] and NCSE-02 Spanish codes, and has a ductility of four. Finally, the third building is also designed using moment-resisting RC frames, but according to the American Concrete Institute (ACI)[21] specifications in order to fulfil ductility requirements of eight. The capacity curve of the WSFB is compared with those of the two MRFB. Fragility curves and damage probability matrices are also obtained in order to compare the probability the WSFB and MRFB exceed different predefined damage states. Preliminary conclusions on the suitability of using WSFB in seismic areas are finally given.

2. DESCRIPTION OF THE BUILDINGS STUDIED

2.1. Building with waffled-slab floors
The WSFB slabs have ribs oriented in two orthogonal directions and a solid thin RC layer in the upper face. The configuration of the ribs generates square spaces on the lower face of the slab, often formed by the use of metal or fibreglass pans or filled with hollow lightweight blocks (see Figure 1).

Slabs bear directly on columns; in order to avoid stress concentration, they have a solid RC element of transition, called solid head, between the ribs and columns (see Figures 2(a) and 2(b)). Solid heads are reinforced in two directions, but also have additional reinforcement aiming to avoid the punching failure at the proximity of the joints.

The WSFB under study has three stories: the first one is 4·5 m high, whereas the other two are 3·0 m high; this is a typical configuration for a building whose ground floor is intended for commercial use. Slab thickness is 30 cm. A typical plan of this building is shown in Figure 3. Reinforcement details of this building are provided in the Appendix.

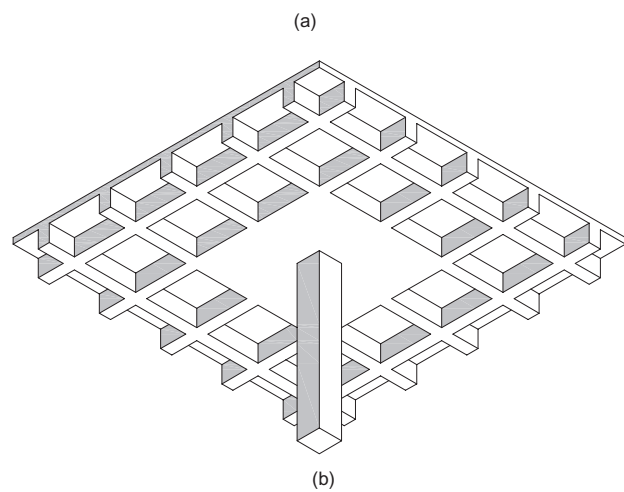Figure 1. View of a waffled-slab floor in construction process

(a)

(b)

Figure 2. (a) Typical waffled-slab floor RC building constructed in Spain; (b) WFSB structural components (viewed from below)

2.2. RC moment-resisting frame buildings
Two RC buildings were designed with the objective of studying the MRFB response: one according to the EHE and NCSE-02 Spanish codes; the second one according to ACI-318 and IBC-2003 codes. Buildings have one-way ribbed slabs and seismic design criteria are added to increase the cross-section size of the columns, thereby yielding a structure with strong columns and weak beams. Further information about the geometry and reinforcement details of buildings can be seen in the Appendix. The characteristics of the materials of the three buildings are

(a) compressive concrete cylinder strength: 25 N/mm² (EHE) and 28 N/mm² (ACI-318)
(b) axial and shear yield strength of steel: 500 N/mm² (EHE) and 525 N/mm² (ACI-318).

2.3. Seismic design of the buildings
Seismic design of the buildings was performed using the inelastic spectrum prescribed by the NCSE-02 Spanish code for stiff soils and basic acceleration of 0·23 g (see Figure 4).
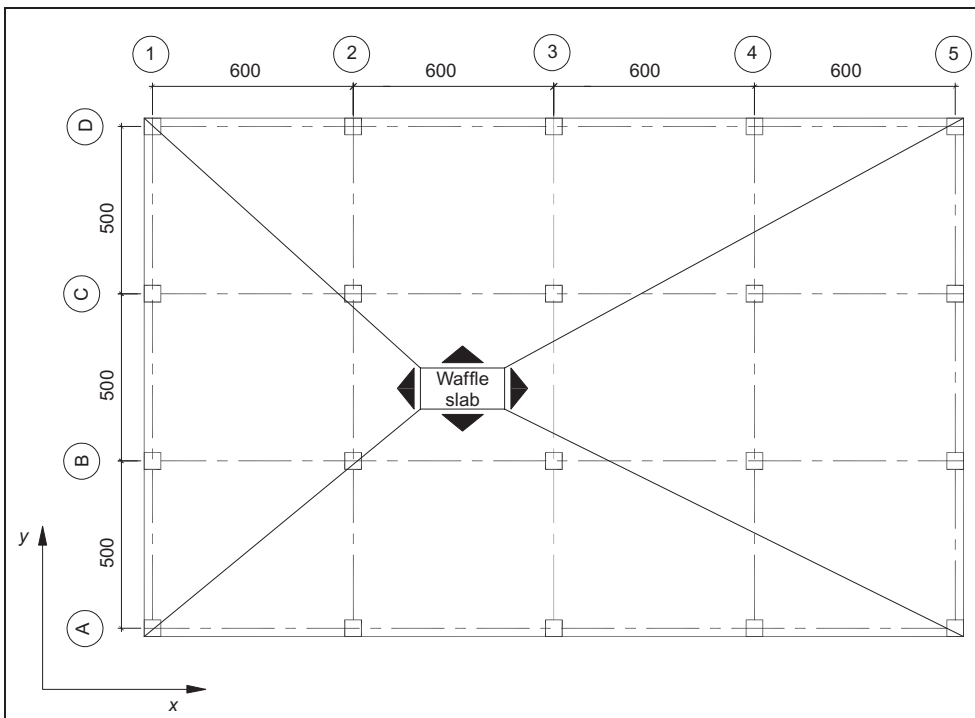
Figure 3. Plan view of the WSFB (dimensions in cm)

Figure 4. Elastic and inelastic spectrum used to perform dynamic analyses

Mode	Period: s		
	WSFB	MRFB (EHE/NCSE-02)	MRFB (ACI-318/IBC-2003)
I	0·93	0·45	0·41
2	0·91	0·44	0·38
3	0·82	0·39	0·37
4	0·27	0·16	0·30
5	0·26	0·16	0·29
6	0·23	0·14	0·23
7	0·12	0·09	0·22
8	0·11	0·09	0·20
9	0·10	0·08	0·17

Table 1. Periods of the modes considered in buildings analyses

Seismic actions were calculated from the three-dimensional (3D) modal analysis, in which three degrees of freedom for level were considered. Table 1 shows modal periods for the three buildings studied.

3. PUSHOVER ANALYSIS

Buildings designed according to the linear elastic methods outlined in the seismic design codes have been studied using a push-over analysis. A single equivalent frame was modelled for each building. For the WSFB the equivalent frame is defined following the recommendations outlined in the ACI-318 code, with three main assumptions.

(a) An equivalent frame is a two-dimensional (2D) frame defined by cutting 3D building along lines midway between columns. For lateral load analyses, the frame must include all floors.
(b) Only 75% of the factored live load is recommended.
(c) Critical zones are defined between the centrelines of the columns and the face of the solid heads. The critical zone is considered as the thickened section of the floor slab, and its equivalent moment of inertia I_{eq} is obtained by

$$I_{eq} = \frac{I}{1 - (c_2/l_2)}$$

where I is the solid head moment of inertia, c_2 is the column width in the transverse direction and l_2 is that of the solid head; this procedure takes into account the shear failure in the critical zone. The equivalent slab moment of inertia can be calculated from its gross section, obtaining an equivalent depth of 19·45 cm. Details of the equivalent frame are shown in Figure 5.
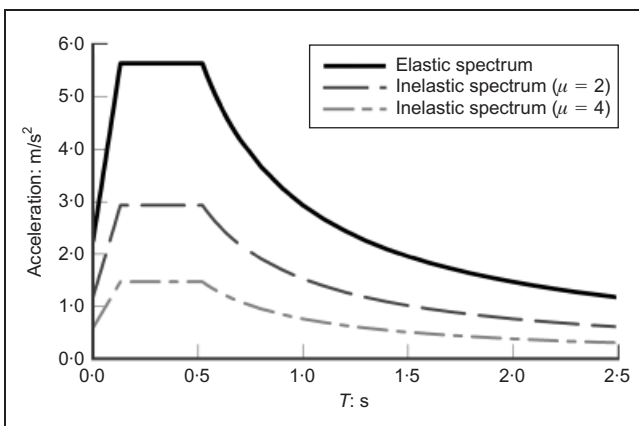
Non-linear static analysis with force control was performed using PLCd[22] finite element code.[23,24] PLCd is a finite element code that works with 2D and 3D solid geometries as well as with prismatic, reduced to one-dimensional (1D) members. This code provides a solution combining both numerical precision and reasonable computational costs.[25,26] It can deal with kinematics and material non-linearities. It uses various 3D constitutive laws to predict the material behaviour (elastic, visco-elastic, damage, damage-plasticity, etc.[27]) with different yield surfaces to control their evolution (Von-Mises, Mohr–Coulomb, improved Mohr–Coulomb, Drucker–Prager, etc.[28]). Newmark's method[29] is used to perform the dynamic analysis. A more detailed description of the code can be found in Mata et al.[25,26] The main numerical features included in the code to deal with composite materials are
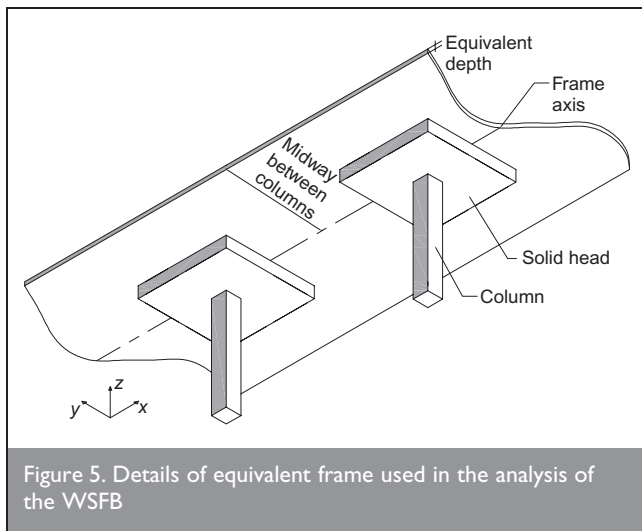
Figure 5. Details of equivalent frame used in the analysis of the WSFB

(*a*) classical and serial/parallel mixing theory used to describe the behaviour of composite components[30]
(*b*) anisotropy mapped space theory enables the code to consider materials with a high level of anisotropy, without the associated numerical problems[24,31]
(*c*) Fibre–matrix debonding which reduces the composite strength due to the failure of the reinforced–matrix interface.[32]

Experimental evidence shows that inelasticity in beam elements can be formulated in terms of cross-sectional quantities[33] and, therefore, the beam's behaviour can be described by means of concentrated models, sometimes called plastic hinge models, which localise all the inelastic behaviour at the ends of the beam by means of ad hoc force–displacement or moment–curvature relationships.[34] In the formulation used in this computer program, however, the procedure consists of obtaining the constitutive relationship at cross-sectional level by integrating on a selected number of points corresponding to fibres directed along the beam's axis.[35]

So, the general non-linear constitutive behaviour is included in the geometrically exact non-linear kinematics formulation for beams proposed by Simo,[25] considering an intermediate curved reference configuration between the straight reference beam and the current configuration. The displacement-based method is used for solving the resulting non-linear problem. Plane cross-sections remain plane after the deformation of the structure; therefore, no cross-sectional warping is considered, avoiding including additional warping variables in the formulation or iterative procedures to obtain corrected cross-sectional strain fields. An appropriated cross-sectional analysis is applied for obtaining the cross-sectional forces and moments[25] and the consistent tangential tensors in the linearised problem. Thermodynamically consistent constitutive laws are used in describing the material behaviour for these beam elements, which allows obtaining a more rational estimation of the energy dissipated by the structures. The simple mixing rule for composition of the materials is also considered in modelling materials for these elements, which are composed by several simple components. Special attention is paid to obtain the structural damage index capable of describing the load-carrying capacity of the structure.

According to the mixing theory, in a structural element coexist N different components, all of them subject to the same strain; therefore, strain compatibility is forced among the material components. Free energy density and dissipation of the composite are obtained as the weighted sum of the free energy densities and dissipation of the components, respectively. Weighting factors k_q are the participation volumetric fraction of each compounding substance, $k_q = V_q/V$, which are obtained as the quotient between the qth component volume, V_q, and the total volume, V.[23–26]

Discretisation of frames was performed with finite elements whose lengths vary depending on the column and beam zones with special confinement requirements, as can be seen in Figure 6. These confinement zones were designed according to
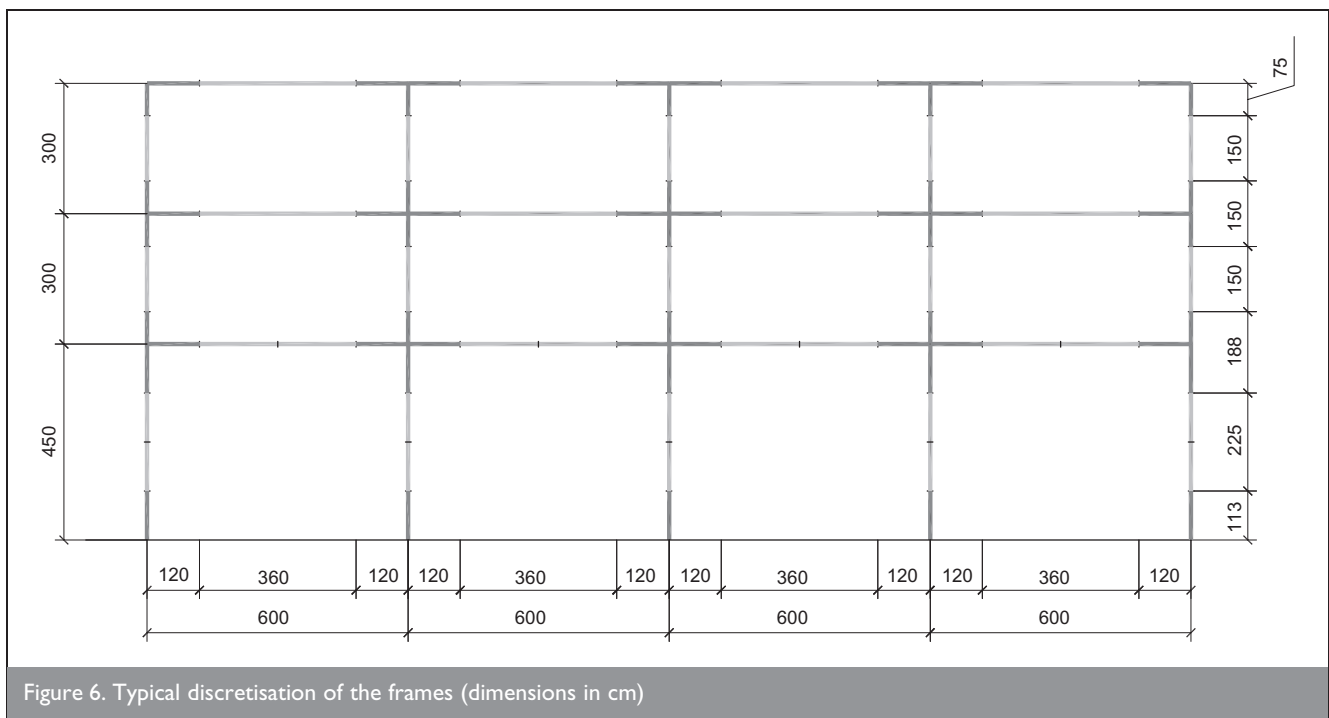

Figure 6. Typical discretisation of the frames (dimensions in cm)

the general dimensions of the structural elements, the diameters of the longitudinal steel, the clear of spans and the storey heights. Frame elements are discretised into equal thickness layers with different composite materials, characterised by their longitudinal and transversal reinforcement ratio (see Figure 7). Transversal reinforcement benefits are included by means of the procedure proposed by Mander *et al.*[36]

The pushover analysis has been performed by applying a set of lateral forces corresponding to the seismic actions in the first vibration mode shape. Lateral forces are gradually increased starting from zero, passing through the value inducing transition from elastic to plastic behaviours and, finally reaching the value which corresponds to the ultimate drift (i.e. the point at which the structure can no longer support any additional load and collapses). Before the structure is subjected to the lateral loads simulating the seismic action, it is first loaded with the gravity loads.

The non-linear static response obtained by way of finite element techniques is used to generate the idealised elasto-plastic behaviour shown in Figure 8, which has a secant segment from its origin to a point (Δ_y, V_y), V_y being the 75% of maximum base shear.[19] The second segment, representing the branch of plastic behaviour, is obtained by finding the intersection of the aforementioned segment with the horizontal corresponding to the maximum base shear. The use of the area compensation procedure guarantees that the energies dissipated by the ideal and the modelled systems are equal, leading to determine Δ_y and Δ_u (see Figure 8) and, consequently, it is possible to obtain the ductility value. In Figure 8, V_d is the design base shear.

The variables which characterise in a simplified way the quality of the building seismic behaviour are the structural ductility, μ, defined as

2	$$\mu = \frac{\Delta_u}{\Delta_y}$$

where Δ_u is the ultimate drift obtained from the idealised capacity curve, and the overstrength R_R of the building, defined as

3	$$R_R = \frac{V_y}{V_d}$$

where V_d is the design base shear and V_y is the yielding base shear (see Figure 8). The design base shear has been calculated using the procedure prescribed in most of the main seismic codes, applying the criteria of the square root of the sum of squares (SRSS) of the values of the forces obtained from modal analysis. Next, the design base shear is normalised respecting the total seismic weight of the structure. Overstrength R_R is similar to a safety factor applied in the design.

4. WSFB NON-LINEAR RESPONSE

The WSFB is designed according to the NCSE-02 and EHE Spanish codes for a structural ductility equal to two. Its capacity curve is calculated using a mechanical model similar to the equivalent frame defined in the ACI-318 code and it is shown in Figure 9(a). Analysis is performed by means of the finite element method and using damage and plasticity constitutive models, as well as the mixing theory.[22–25,27,37] To control the energy dissipation and ensure the correct behaviour of the structure, appropriate mean values of strength and facture energy were used for each compounding material (i.e. steel and concrete).

Structural ductility for the exterior frame is obtained from the yielding drift value Δ_y, and the ultimate drift Δ_u, which can be seen in the idealised capacity curve of Figure 9(a)

Figure 7. Scheme of frame elements

Figure 8. Scheme for determining the damage index of a structural element
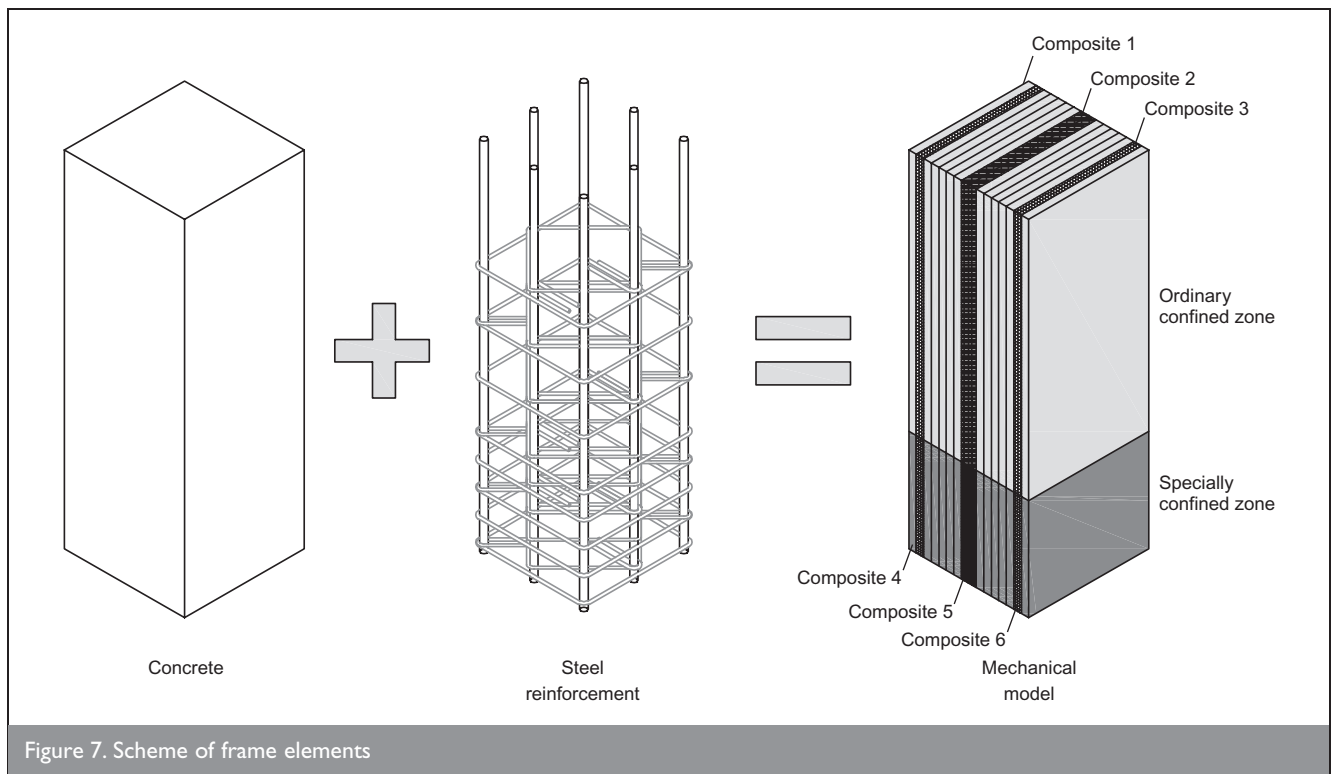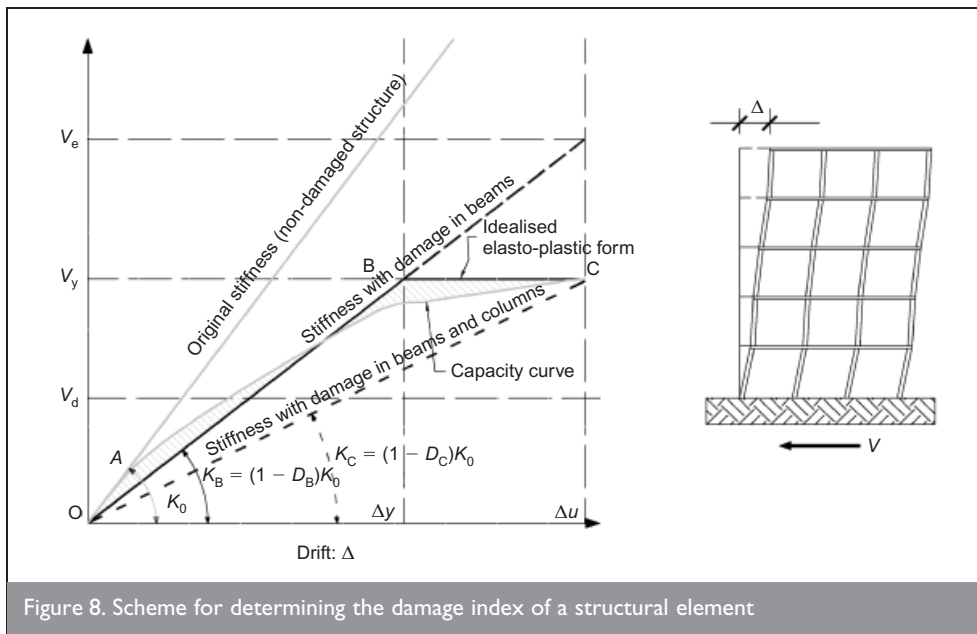
ductility values in the NCSE-02 earthquake-resistant code should be revised. Nevertheless, it is necessary to point that WSFB exhibit high overstrength level.

Figure 9(b) shows the evolution of the damage index for the studied waffled-slab floor building, quantifying stiffness loss in the structural elements resisting loads or the loads leading to failure. This index is calculated using the finite element program PLCd with a constitutive damage and plasticity model that enables correlation of damage with lateral displacements [30,38,39]
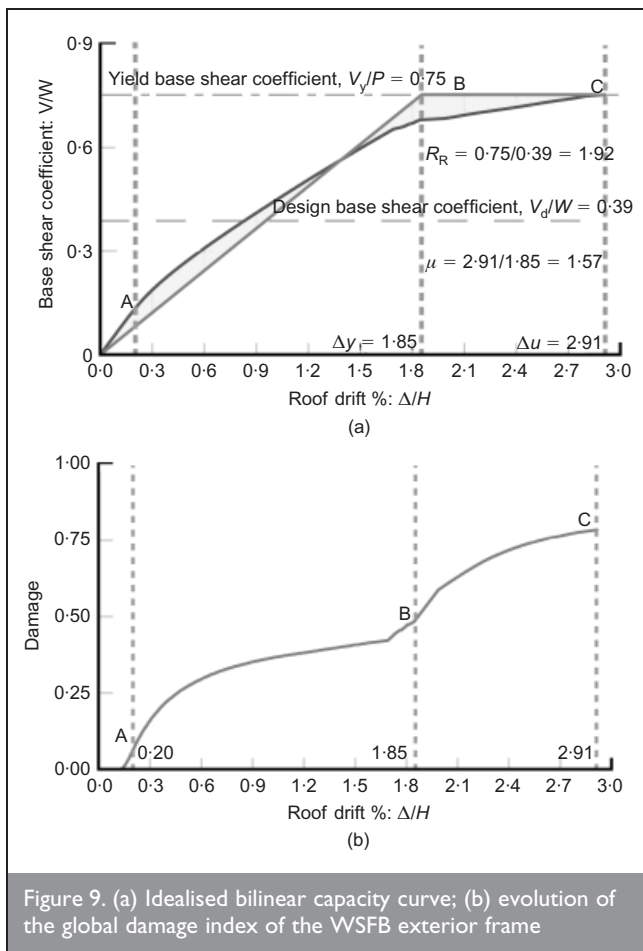

Figure 9. (a) Idealised bilinear capacity curve; (b) evolution of the global damage index of the WSFB exterior frame

$$\begin{array}{c|c} 4 & D = 1 - \dfrac{\|P^{\text{in}}\|}{\|P_0^{\text{in}}\|} \end{array}$$

where $\|P^{\text{in}}\|$ and $\|P_0^{\text{in}}\|$ are the norm of current and elastic values of the internal forces vectors, respectively. Initially, the material remains elastic and $D = 0$, but when all the energy of the material has been dissipated $\|P^{\text{in}}\| \to 0$ and $D \to 1$.

Figure 9(b) indicates the formation of the first micro-cracks in the structure (point A) which increases until plastic hinges appear at the ends of beams, expanding until the appearance of cracks in the columns (point B) and then hinges appear at the ends of the columns. Finally, the ultimate drift threshold is reached (point C). It is of scientific and practical interest to correlate the capacity curve of Figure 9(a) with the damage curve of Figure 9(b). In the case of WSFB, it can be seen how the global damage index of the structure corresponding to the ultimate drift is of 77·5%.

The WSFB low ductility response can be attributed to the formation of plastic hinges in the transition points between the solid head and the slab ribs at the first floor. Slab elements are subjected to bending induced by gravity loads, as well as to the demands of seismic forces; hence, the zones requiring special reinforcement are those closest to the slab–column node and to the middle of the span, where the greatest bending moments frequently appear. Efficient confinement in the central slab zone is, however, technically complicated. This suggests the existence, during earthquakes, of a possible mechanism of structural failure, at the transition zone between the solid slab and the ribs, and consequently, a low level of structure ductility (see Figure 10).

5. MRFB NON-LINEAR RESPONSE

The capacity curve of the MRFB designed according to the EHE and NCSE-02 Spanish codes is shown in Figure 11(a). The curve clearly illustrates how this structural type is capable of sustaining a stable ductile response, which is reflected in the high value of the ultimate drift. Based on the idealised bilinear
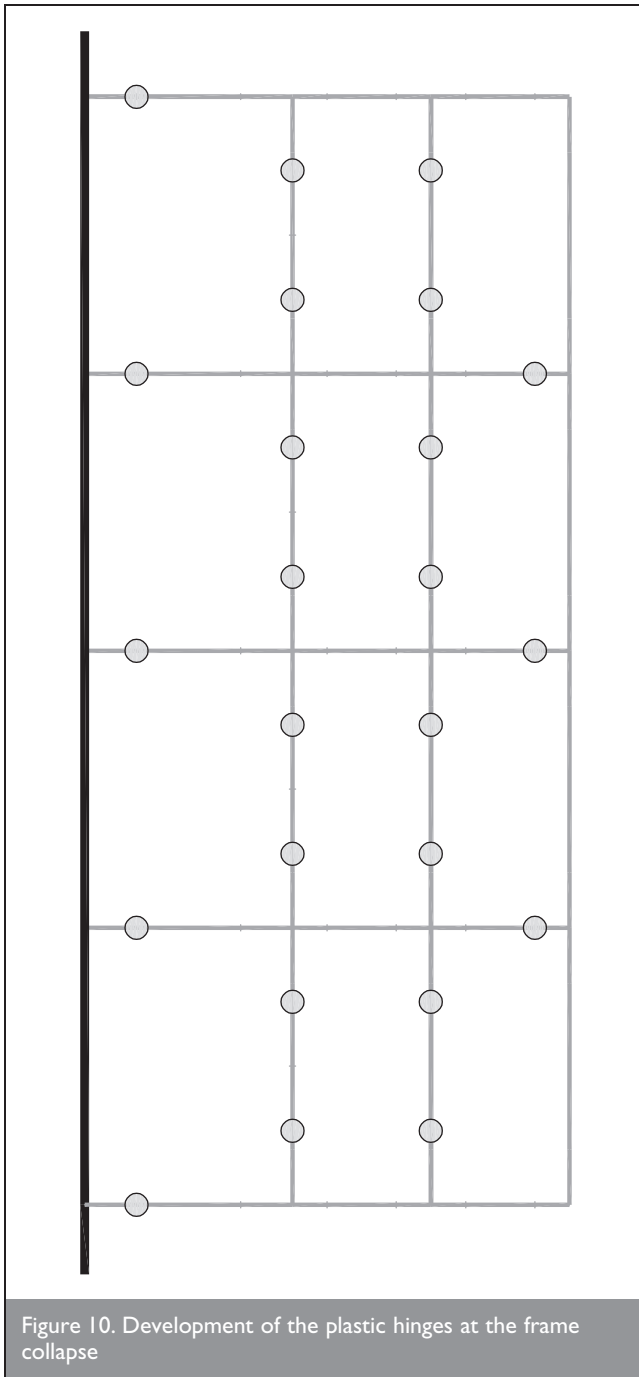
$$\mu = \frac{\Delta_{\text{u}}}{\Delta_{\text{y}}} = \frac{2\cdot91}{1\cdot85} = 1\cdot57$$

The value obtained is very low, even when compared with design value $\mu = 2$ foreseen in the NCSE-02 Spanish code for this structural type. The overstrength is: $R_{\text{R}} = \frac{V_{\text{y}}}{V_{\text{d}}} = 1\cdot92$. Ductility values calculated for this structural class are similar to those obtained for flat slab buildings [12] and suggest that the

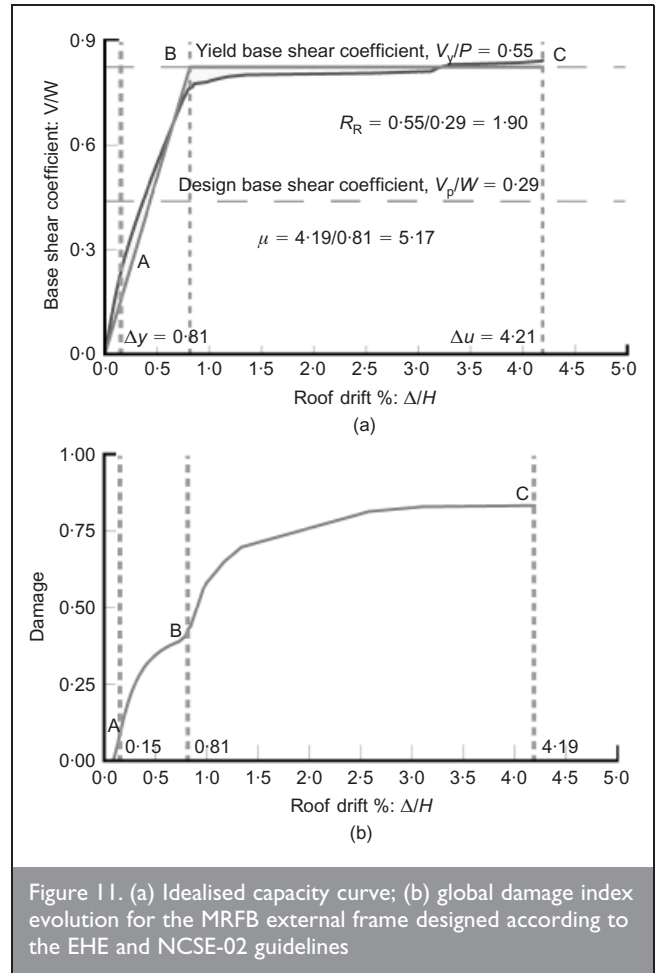Figure 10. Development of the plastic hinges at the frame collapse

Figure 11. (a) Idealised capacity curve; (b) global damage index evolution for the MRFB external frame designed according to the EHE and NCSE-02 guidelines

curve of Figure 11(a), a ductility of 5·17 is obtained; this is a higher value than the one considered in the design, which is 4. This means that MRFB has a ductile response to seismic forces, as well as an adequate overstrength. Figure 11(b) shows the evolution of the global damage index for this type of building, with a maximum damage index of 82% corresponding to the ultimate roof drift.

Figures 10(a) and 10(b) show the capacity curve and the evolution of the damage, respectively, for the external frame of the building designed according to the ACI-318. The main difference between this building and the former is, on the one hand, that the Spanish NCSE-02 earthquake-resistant code limits to four the ductility for this class of buildings to four and, on the other hand, that this code requires less transversal and longitudinal reinforcement than the ACI-318 (2005). At the

same time, the details prescribed in the ACI-318 enable a greater dissipation capacity.

The non-linear response of the ACI-318 moment-resisting frame building is typical for RC low-rise buildings, which generally undergo plastic hinges at the base of their ground floor columns. This general tendency stems from the fact that designing buildings with strong columns and weak beams is not trivial, primarily owing to the predominance of gravitational loads on the beams, which ultimately require larger cross-sections than those of the columns. Figure 12(b) shows that in this case the structure maximum global damage index is 93%.

The above mentioned procedure has been validated by means of non-linear dynamic analyses. The dynamic procedure consists of applying sinusoidal ground acceleration with a peak value scaled with respect to gravity acceleration and increased until yielding is reached. Results obtained shows that the static non-linear procedure allows for accurate calculation of displacements, and that the non-linear dynamic response of the WSFB under study shows a clear pinching behaviour, see Figure 13(b).

6. FRAGILITY CURVES AND DAMAGE PROBABILITY MATRICES

In order to evaluate the non-linear behaviour of the buildings, the performance points were calculated by applying the N2 procedure.[40] The performance points are defined as the intersection of the capacity spectrum (obtained from the
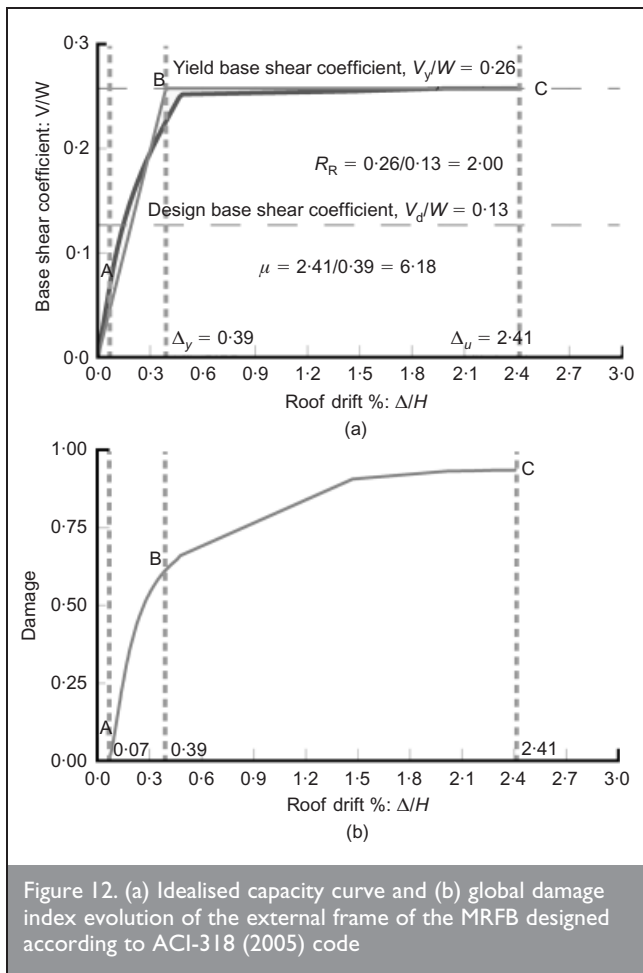
Figure 12. (a) Idealised capacity curve and (b) global damage index evolution of the external frame of the MRFB designed according to ACI-318 (2005) code

capacity curve) with the inelastic demand spectrum (obtained from the elastic design spectrum). Only two cases are included because the non-linear behaviours of the MRFB designed according to EHE and NCSE-02 are very similar to that of the one designed according to ACI-318. The seismic demand is obtained from the elastic spectrum prescribed by NCSE (see Figure 4). Roof drifts are transformed into spectral displacements through the equation

$$5 \qquad S_d = \frac{\delta_c}{MPF}$$

where S_d is the spectral displacement, δ_c is the roof drift and MPF is the modal participation factor corresponding to first mode. Values of the spectral displacements obtained for the performance point are shown in Table 2.

Figures 14 and 15 show the capacity curves of each building together with the stiffness corresponding to initial undamaged state, to performance point and to ultimate drift. It can be observed how close performance and ultimate drift points are in the case of WSFBs.

Damage thresholds are determined using the of Vision 2000 procedure which expresses the thresholds in function of interstorey drifts. Damage-states thresholds are determined from both interstorey drift curve and capacity curve. Slight damage state is defined as the roof drift corresponding to the first plastic hinge. The moderate damage state corresponds to the roof drift for which an interstorey drift of 1% is reached at
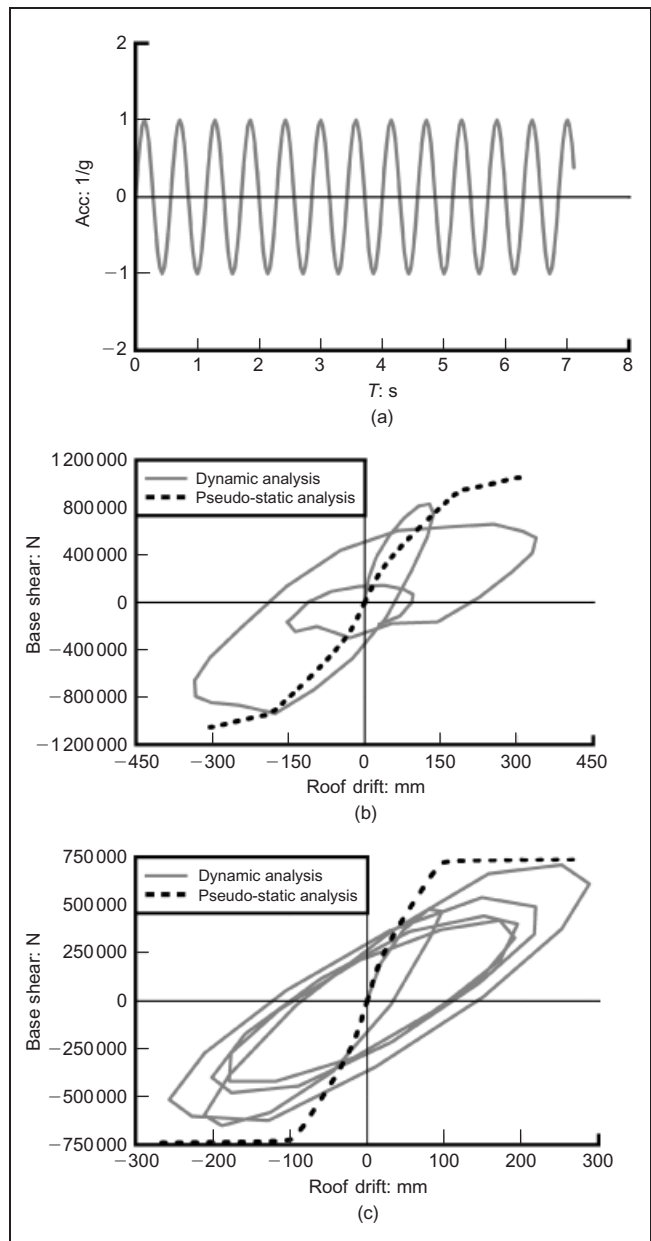

Figure 13. Dynamic response of the two buildings designed according to the NCSE-02: (a) applied sinusoidal excitation; (b) WSFB and (c) MRFB

Building	Roof drift of the performance point: mm
WSFB	222·07
MRFB	120·18

Table 2. Roof drift corresponding to the performance points of the studied buildings

each level. Severe damage state is identified by a roof drift which produces a 2·5% of interstorey drift at each level. Finally, the total damage state (collapse) corresponds to the ultimate roof displacement obtained from the capacity curve. Values of the mean and standard deviation of the roof drift normalised with respect to the building height are shown in Table 3.

Fragility curves are obtained by considering a lognormal

Limit state	WSFB		MRFB	
	Mean	Standard deviation	Mean	Standard deviation
Slight damage	0·22	0·03	0·16	0·02
Moderate damage	0·67	0·04	0·93	0·05
Severe damage	1·67	0·11	2·06	0·10
Collapse	2·91	0·16	4·19	0·14

Table 3. Mean values and standard deviation of the normalised roof drift for limit states

probability density function for the spectral displacements defining damage states

$$
6 \qquad F(S_d) = \frac{1}{\beta_{ds} S_d \sqrt{2\pi}} \exp\left[-\frac{1}{2} \left(\frac{1}{\beta_{ds}} \ln \frac{S_d}{\overline{S}_{d,ds}} \right)^2 \right]
$$

where $\overline{S}_{d,ds}$ is the mean value of spectral displacement for which the building reaches the damage-state threshold d_s and β_{ds} is the standard deviation of the natural logarithm of the spectral displacement for damage state d_s. The conditional probability $P(S_d)$ of reaching or exceeding a particular damage state d_s, given the spectral displacement S_d, is defined as

$$
7 \qquad P(S_d) = \int_0^{S_d} F(S_d)\,d(S_d)
$$

Figures 16 and 17 show fragility curves calculated for WSFB and MRFB, respectively.

Damage probability matrices are obtained by entering the spectral displacement corresponding to the performance point into the fragility curves. The values obtained represent the exceeding probabilities of a damage state and are given in Table 4 for the WSFB and MRFB considered in the analysis.

Table 4 shows that, for the demand being considered, there is a high probability that the limited ductility buildings exceed the severe damage state and the collapse state. Severe damage state exceeding probability is of 36·2% for the WSFB. The collapse
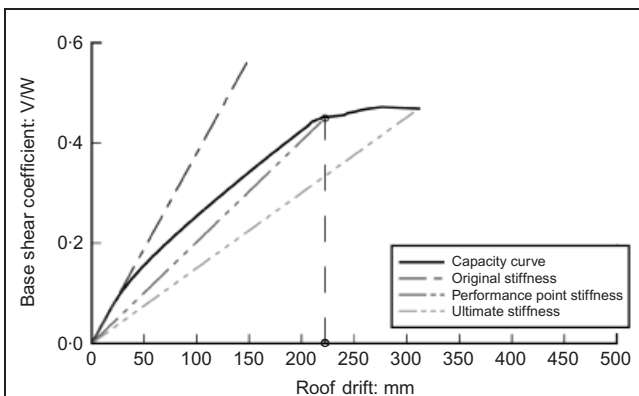

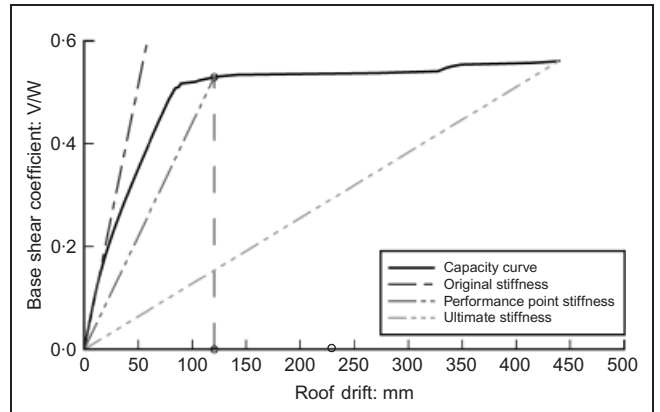Figure 15. Roof drift corresponding to the performance point of the building with moment- resisting frames (NCSE-02 code)

	WSFB	MRFB
No damage	0·2%	0·4%
Slight	9·4%	40·3%
Moderate	24·6%	44·4%
Severe	36·2%	13·9%
Collapse	29·6%	1·0%

Table 4. Damage probability matrices for the studied building typologies

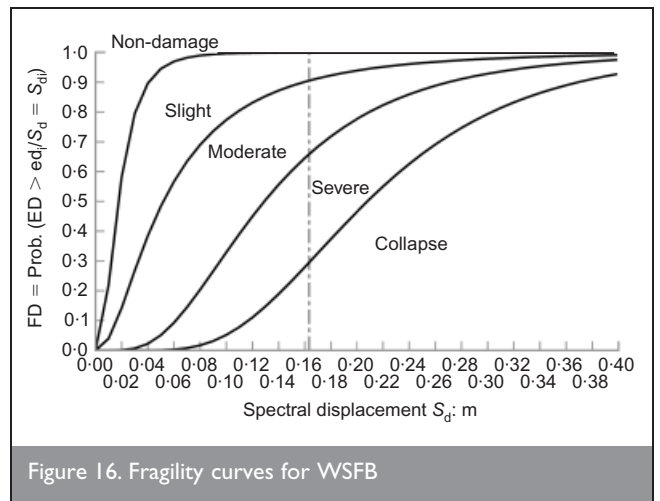Figure 16. Fragility curves for WSFB

Figure 14. Roof drift corresponding to WSFB performance point

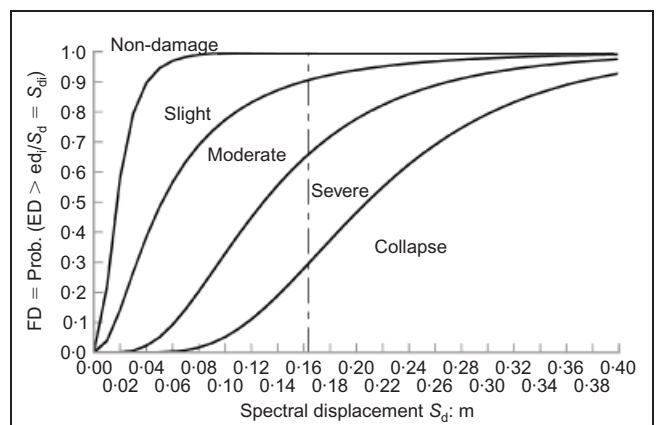

Figure 17. Fragility curves for MRFB designed according to the Spanish codes

probabilities are 29·6% for the WSFB and only about 1% for the MRFB.

7. POSSIBILITIES OF IMPROVING THE SEISIMC RESPONSE OF WSFBS

Figure 18 shows the capacity curves corresponding to all cases under study. Design base shears have also been plotted in this figure, in which it is evident that each of the three buildings has base shear coefficients greater than the design one, indicating that they satisfy this initial design objective. However, overstrength varies dramatically among the three structures. It is interesting to compare the MRFB capacity curves, which have similar structural typology but are designed with different codes and thus their reduction factors differ. Both exhibit ductility several times higher than that of the WSFB while providing satisfactory overstrength.

Results of the WSFB non-linear analysis raise this question; can their response be improved at design stage, in order to reach the ductility values prescribed in the NCSE-02 code maintaining the same structural typology? This section discusses this possibility based on the pushover analysis performed using the finite element method and comparing responses obtained with those corresponding to the MRFB. For the purpose of studying the influence of the steel type on the WSFB non-linear response, steels with different mechanical characteristics are considered. Buildings are calculated by considering the reinforcement with either weldable-ductile steel (WD), whose characteristics make it recommendable for the

earthquake-resistant design of structures according to the EHE and Eurocode 8 specifications, or weldable steel (W) (see Table 5). For both cases, the yielding stresses B 400 and B 500 steel were considered (see Figure 19).

Results of the pushover analysis are shown in Figure 19, which reveals that frames reinforced with ductile steel have only a slightly more ductile response than do those reinforced with non-ductile steel. Hence, the building global response is influenced to a much greater extent by the general configuration and structural typology chosen than by the characteristics of the reinforcement steel.

Finally, Figure 20 shows the same results obtained for the MRFB reinforced with different types of steel. Observe that, in
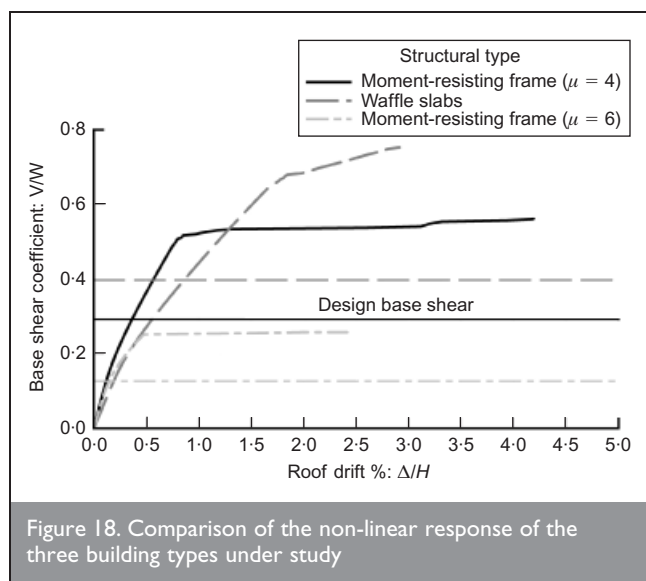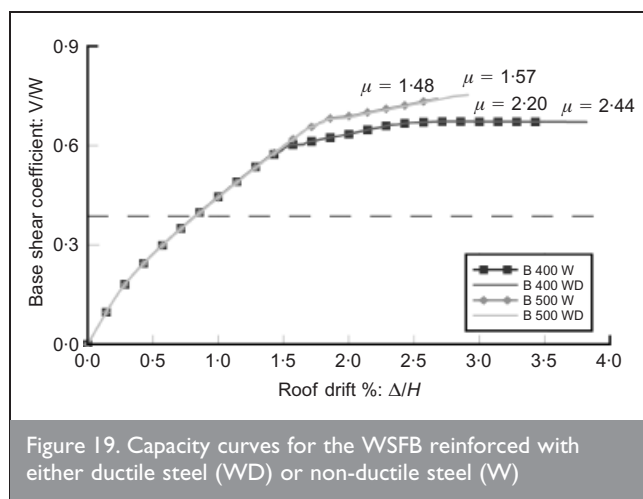

Figure 19. Capacity curves for the WSFB reinforced with either ductile steel (WD) or non-ductile steel (W)

Figure 18. Comparison of the non-linear response of the three building types under study
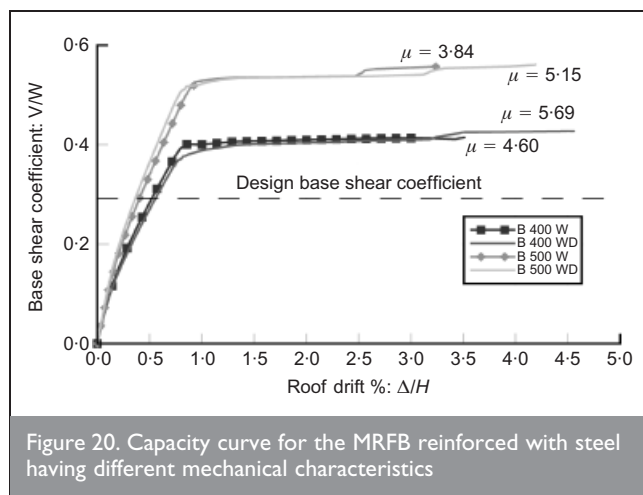

Figure 20. Capacity curve for the MRFB reinforced with steel having different mechanical characteristics

| Steel type | Eurocode 8 | | EHE | |
	B	C	B 400 WD	B 500 WD
Yield stress f_y: N/mm^2	400–600	400–600	400	500
Ultimate stress f_s: N/mm^2	—	—	480	575
Ratio f_s/f_y	⩾ 1·08	⩾ 1·15 and ⩽ 1·35	⩾ 1·20 and ⩽ 1·35	⩾ 1·15 and ⩽ 1·35
Maximum strain ε_{max}: %	⩾ 5·0	⩾ 7·5	⩾ 9·0	⩾ 8·0
Ultimate strain, ε_u: %	—	—	⩾ 20·0	⩾ 16·0

Table 5. Characteristics of the steel recommended by Eurocode 8 and by EHE for the design of ductile reinforced concrete buildings

this case, increasing the steel ductility leads to a major increase in structural ductility.

8. CONCLUSIONS

(a) The WSFB seismic behaviour has been studied using the pushover analysis with force control. In order to determine the structure ultimate drift threshold, global damage index must approximate to a value of 0·8. Yielding drifts of the structures are obtained using the idealised bilinear capacity curves proposed by Park.

(b) Among the cases studied only the MRFB exhibit sufficient ductility and overstrength to guarantee a stable behaviour, showing ductility values higher than those of the design.

(c) It has been proved in this paper that WSFB should be designed for lower ductility levels than those prescribed in the Spanish seismic code (NCSE-02) because the prescribed design values ($\mu = 2$) are greater than the obtained from numerical simulations ($\mu = 1\cdot57$). Nevertheless, during earthquakes, WSFB show adequate overstrength.

(d) It can also be seen that the exceeding probabilities for the MRFB damage states are lower than those of WSFB.
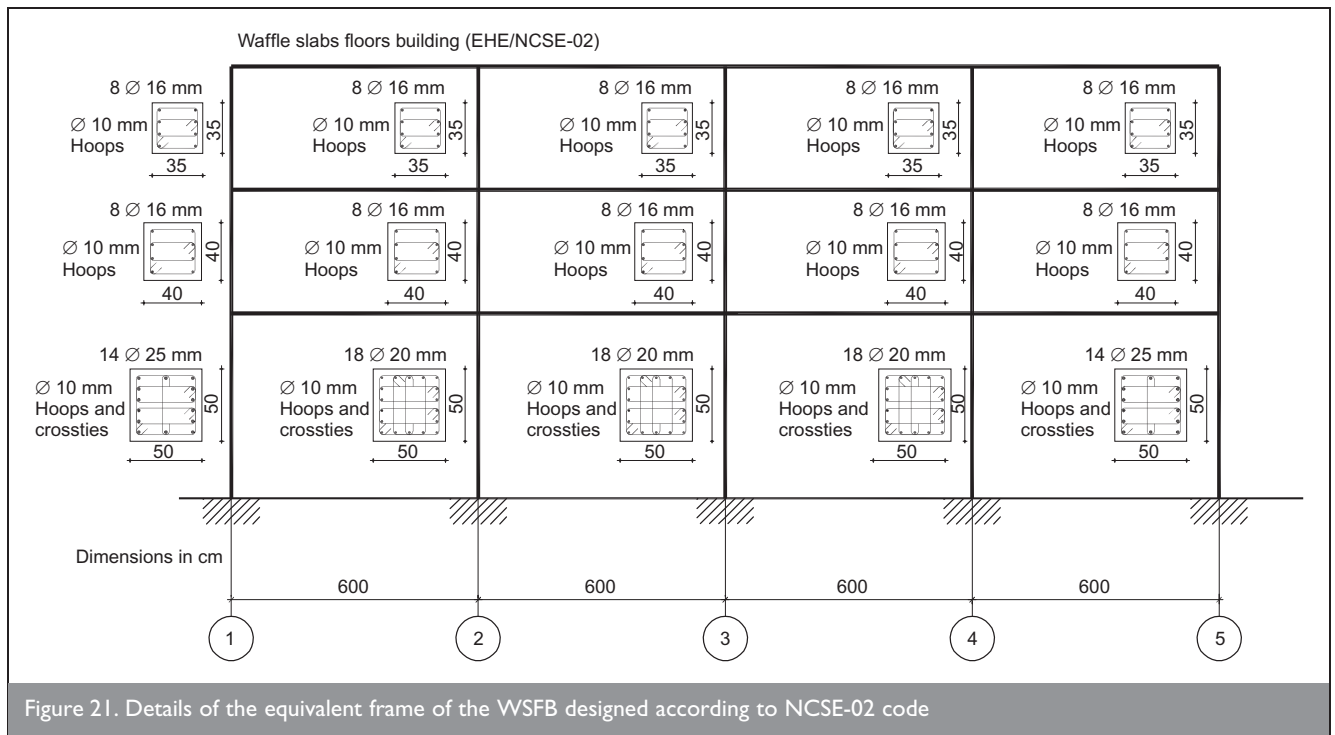
(e) Structural response of the WSFB cannot be improved using better mechanical characteristics of materials or a better confinement of their members.

(f) The only possibility of improving the WSFB behaviour is to add depth beams to in order to increase their lateral stiffness.

APPENDIX

Reinforcement details of the three studied buildings

Figure 21. Details of the equivalent frame of the WSFB designed according to NCSE-02 code

Plan view

Edge beam · Column · Solid head

70
10
70
10

70 · 70 · 70 · 70
10 · 10 · 10 · 10 · 10

Ribs

Details of reinforcement

Top bars
8 ∅ 10 mm

Bottom bars
8 ∅ 10 mm

Top bars
4 ∅ 10 mm

Bottom bars
2 ∅ 10 mm

Dimensions in cm

Edge beam

2 ∅ 16 mm
30
2 ∅ 12 mm
25
∅ 6 mm
Hoops @ 20

Ribs reinforcement

2 ∅ 16 mm
2 ∅ 16 mm

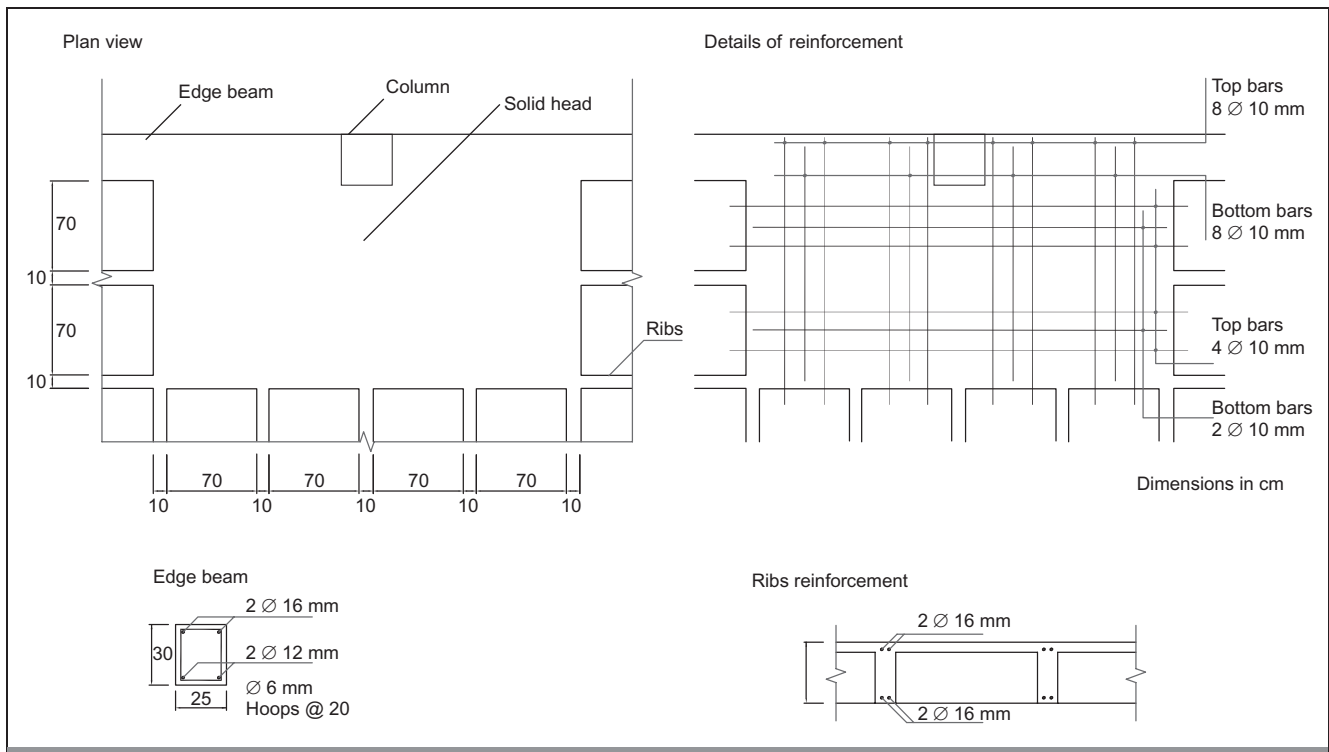**Figure 22. Details of the reinforcement of the solid head and waffle slab**

Moment-resisting framed building (EHE/NCSE-02)

6 ∅ 16 mm
∅ 10 mm
Hoops and
crossties
30 × 30

6 ∅ 16 mm
∅ 10 mm
Hoops and
crossties
30 × 30

6 ∅ 16 mm
∅ 10 mm
Hoops and
crossties
30 × 30

6 ∅ 16 mm
∅ 10 mm
Hoops and
crossties
30 × 30

6 ∅ 16 mm
∅ 10 mm
Hoops and
crossties
30 × 30

4 ∅ 16 mm
4 ∅ 16 mm
50
30
∅ 10 mm hoops

6 ∅ 20 mm
∅ 10 mm
Hoops and
crossties
35 × 35

6 ∅ 20 mm
∅ 10 mm
Hoops and
crossties
35 × 35

8 ∅ 20 mm
∅ 10 mm
Hoops
35 × 35

6 ∅ 20 mm
∅ 10 mm
Hoops and
crossties
35 × 35

6 ∅ 20 mm
∅ 10 mm
Hoops and
crossties
35 × 35

4 ∅ 20 mm
4 ∅ 16 mm
55
30
∅ 10 mm hoops

6 ∅ 25 mm
∅ 10 mm
Hoops
40 × 40

6 ∅ 25 mm
∅ 10 mm
Hoops and
crossties
40 × 40

8 ∅ 25 mm
∅ 10 mm
Hoops
40 × 40

6 ∅ 25 mm
∅ 10 mm
Hoops and
crossties
40 × 40

6 ∅ 25 mm
∅ 10 mm
Hoops and
crossties
40 × 40

4 ∅ 20 mm
4 ∅ 20 mm
60
30
∅ 10 mm hoops

Dimensions in cm

600 · 600 · 600 · 600

1 · 2 · 3 · 4 · 5

Figure 23. Details of the moment-resisting frame designed according to EHE/NCSE-02 codes

Figure 24. Details of the moment-resisting frame designed according to ACI-318/IBC-2003

Figure 25. Details of the confined zones in columns and beams of the frame designed according to ACI-318/IBC-2003
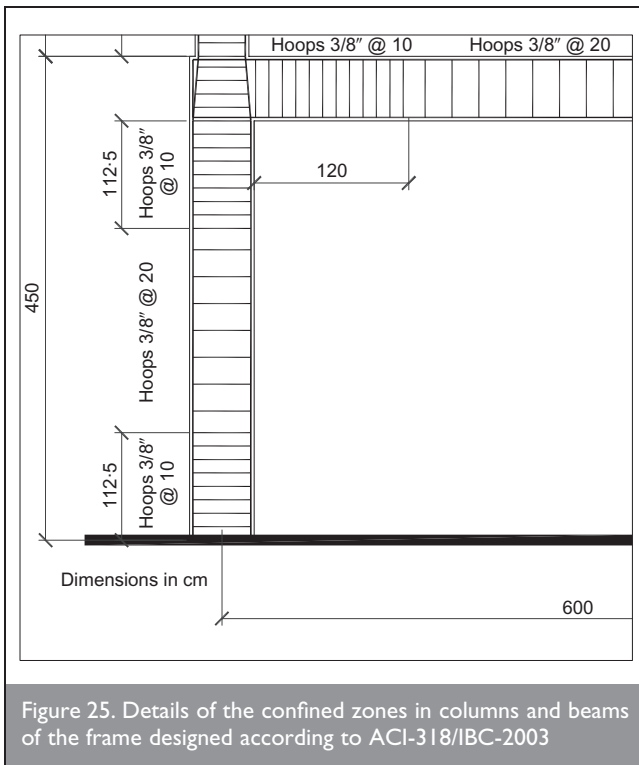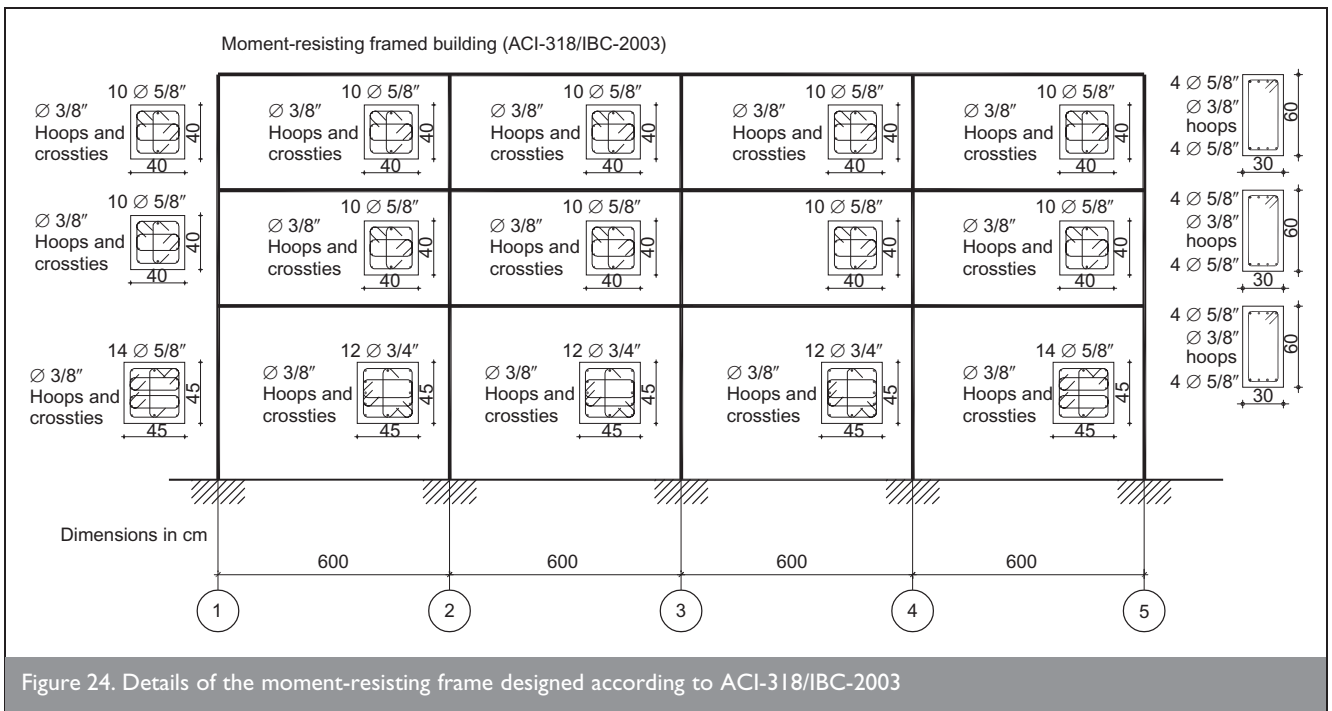
REFERENCES

1. EGOZCUE J. J., BARBAT A. H., CANAS J. A., MIQUEL J. and BANDA E. A method to estimate occurrence probabilities in low seismic activity regions. *Earthquake Engineering and Structural Dynamics*, 1991, **20**, No. 1, 43–60.

2. BARBAT A. H., YÉPEZ MOYA F. and CANAS J. A. Damage scenarios simulation for risk assessment in urban zones. *Earthquake Spectra*, 1996, **2**, No. 3, 371–394.

3. BARBAT A. H., PUJADES L. G. and LANTADA N. Performance of buildings under earthquakes in Barcelona, Spain. *Computer-Aided Civil and Infrastructure Engineering*, 2006, **21**, No. 8, 573–593.

4. BARBAT A. H., PUJADES L. G. and LANTADA N. Seismic damage evaluation in urban areas using the capacity spectrum method: application to Barcelona. *Soil Dynamics and Earthquake Engineering*, 2008, **28**, Nos 10–11, 851–865.

5. SEAOC. *Vision 2000 Report on Performance Based Seismic Engineering of Buildings.* Structural Engineers Association of California, Sacramento, California, 1995, Vol. I

6. APPLIED TECHNOLOGY COUNCIL (ATC). *ATC-40: The Seismic Evaluation and Retrofit of Concrete Buildings.* ATC, Redwood City, CA, 1996.

7. FEDERAL EMERGENCY MANAGEMENT AGENCY. *NEHRP Guidelines for the Seismic Rehabilitation of Buildings.* FEMA 273–Provisions. FEMA 274–Commentary, Washington, DC, 1997.

8. BERTERO R. and BERTERO V. Performance-based seismic engineering: the need for a reliable conceptual comprehensive approach. *Earthquake Engineering and Structural Dynamics*, 2002, **31**, No. 3, 627–652.

9. ELNASHAI A. and MWAFI A. Overstreght and force reduction factors of multistory reinforced-concrete buildings. *Structural Design of Tall Buildings*, 2002, **11**, No. 5, 329–351.

10. FRAGIACOMO M., AMADIO C. and RAJGELJ S. Evaluation of the structural response under seismic actions using non-linear static methods. *Earthquake Engineering and Structural Dynamics*, 2006, **35**, No. 12, 1511–1531.

11. ERBERIK A. and ELNASHAI A. Loss estimation analysis of flat-slab structures. *Journal of Structural Engineering*, 2006, **7**, No. 1, 26–37.

12. HUESTE M B. and BAI J.-W. Seismic retrofit of a reinforced concrete flat-slab structure: Part I —seismic performance evaluation. *Engineering Structures*, 2007, **29**, No. 6, 1165–1177.

13. *Uniform Building Code (UBC-97).* International Building Conference of Building Officials, Whittier, California, 1997.

14. *International Building Code (IBC-2003).* International Building Conference of Building Officials, Whittier, California, 2003.

15. COMITÉ EUROPÉEN DE NORMALISATION. *Eurocode 8: Design of Structures for Earthquake Resistance.* CEN, Brussels, 2003.

16. NORMA DE CONSTRUCCIÓN SISMORRESISTENTE. BOE No. 244. NSCE-2002. Madrid. 2002. Available online from: http://www.proteccioncivil.org/centrodoc/legisla/NCSR-02.pdf.

17. BARBAT A. H., OLLER S. and VIELMA J. C. *Confinement and Ductility of Reinforced Concrete Buildings.* ARCER, monograph No. 5, Madrid, 2007. In Spanish.

18. VIELMA J. C., BARBAT A. H. and OLLER S. Evaluación de la respuesta no lineal de edificios de hormigón armado con ductilidad limitada. *Hormigón y Acero*, 2008, **248**, 55–60.

19. PARK R. State-of-the-art report: ductility evaluation from laboratory and analytical testing. *Proceedings 9th WCEE, IAEE, Tokyo-Kyoto*, 1988, **VIII**, 605–616.

20. COMISIÓN PERMANENTE DEL HORMIGÓN. *Instrucción de hormigón estructura (EHE).* Leynfor siglo XXI, Madrid, 1998.

21. AMERICAN CONCRETE INSTITUTE. *Building Code Requirements for Structural Concrete (ACI 318-05).* ACI, Farmington Hills, Michigan, 2005, ACI Committee 318.

22. PLCd Manual. *Non-linear thermo mechanic finite element oriented to PhD student education.* Code developed at CIMNE, Barcelona, Spain, 2008.

23. OLLER S. and BARBAT A. H. Moment–curvature damage model for bridges subjected to seismic loads. *Computer Methods in Applied Mechanics and Engineering*, 2006, **195**, 4490–4511.

24. CAR E., OLLER S. and OÑATE E. A large strain plasticity for anisotropic materials: composite material application. *International Journal of Plasticity*, 2001, **17**, No. 11, 1437–1463.

25. MATA P., OLLER S. and BARBAT A. H. Static analysis of beam structures under nonlinear geometric and constitutive behaviour. *Computer Methods in Applied Mechanics and Engineering*, 2007, **196**, Nos 45–48, 4458–4478.

26. MATA P., OLLER S. and BARBAT A. H. Dynamic analysis of beam structures under nonlinear geometric and constitutive behaviour. *Computer Methods in Applied Mechanics and Engineering*, 2008, **197**, Nos 6–8, 857–878.

27. OLLER S., ONATE E., OLIVER J. and LUBLINER J. Finite element non-linear analysis of concrete structures using a plastic-damage model. *Engineering Fracture Mechanics*, 1990, **35**, Nos 1–3, 219–231.

28. LUBLINER J., OLIVER J., OLLER S. and OÑATE E. A plastic-damage model for concrete. *International Journal of Solids and Structures*, 1989, **25**, No. 3, 299–326.

29. BARBAT A. H., OLLER S., ONATE E. and HANGANU A. Viscous damage model for Timoshenko beam structures. *International Journal of Solids and Structures*, 1997, **34**, No. 30, 3953–3976.

30. FALEIRO FREITAS J., OLLER S. and BARBAT A. H. Plastic-damage seismic model for reinforced concrete frames. *Computers and Structures*, 2008, **86**, Nos 7–8, 581–597.

31. OLLER S., CAR E. and LUBLINER J. Definition of a general implicit orthotropic yield criterion. *Computer Methods in Applied Mechanics and Engineering*, 2003, **192**, Nos 7–8, 895–912.

32. MARTINEZ X., OLLER S., RASTELLINI F. and BARBAT A. H. A numerical procedure simulating RC structures reinforced with FRP using the serial/parallel mixing theory. *Computers and Structures*, 2008, **86**, Nos 15–16, 1604–1618.

33. BAYRAK O. and SHEIKH S. A. Plastic hinge analysis. *Journal of Structural Engineering*, 2001, **127**, No. 9, 1092–100.

34. SPACONE E. and EL-TAWIL S. Nonlinear analysis of steel–concrete composite structures: State of the art. *Journal of Structural Engineering,* 2000, **126**, No. 2, 159–168.

35. SHAO Y., AVAL S. and MIRMIRAN A. Fiber–element model for cyclic analysis of concrete-filled fiber reinforced polymer tubes. *Journal of Structural Engineering,* 2005, **131**, No. 2, 292–303.

36. MANDER J. B., PRIESTLEY M. J. N. and PARK R. Observed stress-strain behaviour of confined concrete. *Journal of Structural Engineering*, 1988, **114**, No. 8, 1827–1849.

37. HANGANU A., OÑATE E. and BARBAT A. H. A finite element methodology for local/global damage evaluation in civil engineering structures. *Computers and Structures*, 2002, **80**, Nos 20–21, 1667–1687.

38. BARBAT A. H., OLLER S., OÑATE E. and HANGANU A. Viscous damage model for Timoshenko beam structures. *International Journal of Solids and Structures*, 1997, **34**, No. 30, 3953–3976.

39. CAR E., OLLER S. and OÑATE E. An anisotropic elastoplastic constitutive model for large strain analysis of fiber reinforced composite materials. *Computer Methods in Applied Mechanics and Engineering*, 2000, **185**, Nos 2-4, 245–277.

40. FAJFAR P. A Nonlinear analysis method for performance based seismic design. *Earthquake Spectra*, 2000, **16**, No. 3, 573–591.